Multi-scale simulation of degradation of polymer coatings

Polymer Degradation and Stability 123 (2016) 1–12

Contents lists available at ScienceDirect

Polymer Degradation and Stability

journal homepage: www.elsevier.com/locate/polydegstab

Multi-scale simulation of degradation of polymer coatings: Thermo-mechanical simulations

Hesam Makki [a, b], Koen N.S. Adema [a, b], Elias A.J.F. Peters [a], Jozua Laven [a], Leendert G.J. van der Ven [a], Rolf A.T.M. van Benthem [a, c], Gijsbertus de With [a, *]

[a] Laboratory of Materials and Interface Chemistry, Department of Chemical Engineering and Chemistry, Eindhoven University of Technology, Den Dolech 2, 5612, AZ, Eindhoven, The Netherlands
[b] Dutch Polymer Institute (DPI), P.O. Box 902, 5600, AX, Eindhoven, The Netherlands
[c] DSM Ahead Performance Materials BV, P.O. Box 18, 6160, MD, Geleen, The Netherlands

ARTICLE INFO

Article history:
Received 16 September 2015
Received in revised form
19 October 2015
Accepted 4 November 2015
Available online 7 November 2015

Keywords:
Multi-scale simulation
Molecular dynamics
Thermo-mechanical analysis
Structure-property relation
Photo-degradation

ABSTRACT

In this work we simulate the full sequence of steps that are also typically performed in an experimental approach when studying photo-degradation of a polymer coating, namely, i) sample preparation, ii) photo-degradation and iii) thermo-mechanical analysis of the material during photo-degradation. In the current paper, we focus on performing several molecular dynamics simulations to study the thermo-mechanical properties of a virgin thermoset coating as well as degraded ones. Using an atomistic structure that is obtained by fine-graining the mesoscopic structure, we obtain consistent correlations between the simulated thermo-mechanical properties of the material and those measured experimentally. In addition, it is shown that by using oscillatory strain fields in MD - instead of the commonly applied linear tensile/compression strain fields – one can acquire greater knowledge on the structure-property relation of polymeric materials. Eventually, we show that our simulation approach gives rise to a remarkable insight into the mechanism of the photo-degradation process.

1. Introduction

Polymeric coatings are designed for different demands and, accordingly, have to fulfill different requirements. Among these, preserving their functionality during the service life of these coatings is of a great importance. Exposure to the environmental stress factors, i.e., photons, elevated temperature, oxygen and water, for prolonged time leads to macroscopic failure of these coatings, such as (micro) cracks. Accordingly, a keen interest exists in understanding the long-term performance of these coatings, and sophisticated experimental methods such as FTIR [1] and UV–vis spectroscopy [2], ESR [3] and mass spectroscopy [4] techniques are used to characterize their degradation processes.

Due to the fact that organic coatings, particularly clearcoats, are designed to be highly resistant to environmental stress factors, outdoor experimental degradation tests are rather time-consuming. Therefore, “faster” artificial degradation setups, which mimic real outdoor conditions with higher intensity of the stress factors are used, although there is always a fear of deviation from the chemical pathways of degradation for natural exposure because “relatively small variations in weathering performance can lead to significant variations in failure rates at a given time in service” [5]. Moreover, due to the complex chemistry of the photo-degradation processes, in which several stress factors influence the process at the same time, it is difficult to distinguish the effect of each parameter separately.

Although these type of measurements give a wealth of information, a great deal of interpretation is needed to deduce reaction pathways or failure mechanisms. In this respect high quality molecular simulations can provide a more direct view. In addition, simulations offer much more elements of control than experiments. For example, one can artificially allow one possible mechanism to play its role in a degradation simulation, to clarify its role. Finally, by combining experiments and simulation, a deeper mechanistic understanding can be developed. However, there are only a few simulation studies on this topic available in the literature [6–8] despite the extensive experimental investigations on the photo-degradation of polymeric coatings [9–14].

There are generally two approaches for simulation studies on photo-degradation processes in the literature, namely the stochastic approach [5] and mechanistic modeling [7]. Both types of

* Corresponding author.
E-mail address: G.deWith@tue.nl (G. de With).

http://dx.doi.org/10.1016/j.polymdegradstab.2015.11.005
0141-3910/

simulation give insight into changes in the *macroscopic* properties of a coating during the degradation process. In order to assess the *microscopic* aspects of the photo-degradation process via simulation, as required to obtain insight into the structure-property relations of these coatings, one needs to think about the wide time spectrum of different degradation events taking place in the material [8]. This means that the spectrum of time scales in such a simulation should range from picoseconds – the typical time scale of chemical reactions – to years – the time scale before mechanical failure of the material is observable. No single molecular simulation method can cover such a wide spectrum in time; therefore, a multi-scale approach is necessary. The focus of this paper is to justify our multi-scale approach. We also show that our approach is capable of providing the relation between the mechanisms involved and the changes in material's properties.

The material used (Fig. 1) and the conditions for the photo-degradation (under dry nitrogen) employed for our simulations are the same as in a preceding paper [8]. Here, after a brief overview of our multi-scale simulation approach [8] (Section 2), we introduce the additional simulation methods, not covered in the previous paper, that enable us to compute the physical and mechanical properties of the material during the photo-degradation process (Section 3). Thereafter we discuss the results of our study (Sections 4 and 5).

2. The methodology of photo-degradation simulation

Our multi-scale simulation approach consists of four major steps: 1) Building up the cross-linked structure of the virgin material by a coarse-grained method, where molecules are composed of beads that represent groups of atoms [15], 2) performing the photo-degradation simulation, 3) reverse mapping from the coarse-grained (CG) structure to the corresponding atomistic structure of the material, and 4) computing the properties of the degraded material by atomistic methods.

2.1. Network formation

The first step of our approach is constructing a cross-linked polymer network. This is hardly feasible in an atomistically detailed Molecular Dynamics (MD) simulation, due to the large time scale of the cross-linking process in polymers as compared to the time scales that can be attained in MD simulations; therefore, we used a CG method, i.e., Dissipative Particle Dynamics (DPD) [16]. For our study we used a polyester resin with an isocyanurate cross-linker based on hexamethylenediisocyanate. The coarse-graining as used in the DPD method is shown in Fig. 1. Note that we used 5 different beads and 4 different bonds, as such detail is required for the subsequent Kinetic Monte Carlo (KMC) simulations from which the degraded structures are obtained.

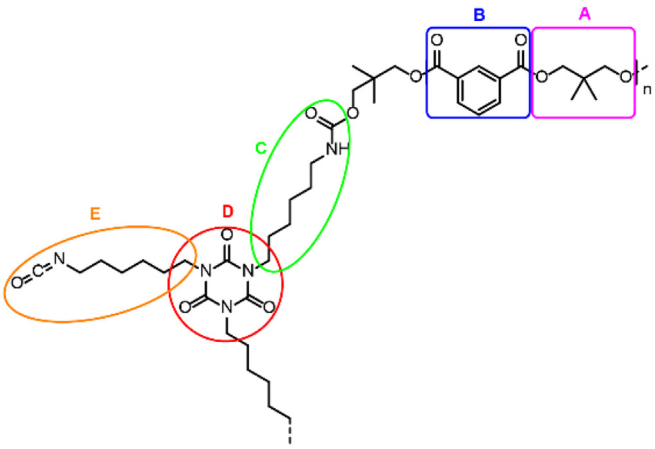

Fig. 1. The atomistic and the corresponding coarse-grained chemical structure of the cross-linked polyester network.

2.2. Photodegradation

For the second step, namely, "photo-degradation simulation", the spectrum of time scales is so large that no time-driven molecular simulation method is able to capture the whole spectrum (from reaction times of typically a few picosecond to the final stage of degradation after several years). Consequently, we developed an event-driven simulation method based on a Kinetic Monte Carlo (KMC) algorithm to capture the chemical pathways of the photo-degradation process. We also showed that it is necessary to couple our event-driven method to a time-driven method in order to allow for structural relaxation of the network during the photo-degradation process [8]. Therefore, we connected our photo-degradation simulation to a DPD simulation to fulfill the structural relaxation requirement of the material [8].

During the photo-degradation simulation, according to the chemical reactions involved (see Fig. 2), different beads and bonds can form. As shown in Fig. 1, the virgin material (the cross-linked polyester at zero degradation time) consists of five different CG beads (from A to E) and four different CG bonds (A–B, B–C, C–D and D–E). As a result of photo-degradation, five other beads (A̛, B̛, C̛, β and β̛) and two other types of bonds (A–A and β–β) can form. Fig. 3 shows a summary of new CG beads and bonds that can evolve during a photo-degradation simulation.

In case study II of a previous paper [8], the reaction rate constants for each set of reactions, i.e., initiation, propagation and termination, were set at 1 dt^{-1}, where for the 'degradation time' $dt = 1$ s was chosen as unit of time. Because the structure was fully relaxed in between subsequent degradation events, the time evolution expressed in dt units will be the same, irrespective of the absolute value of dt. Real differences occur only if rates are changed relative to each other. In this paper, we discuss the results for independently generated samples of the material obtained at four moments in time during the photo-degradation simulation process, namely, 0, 0.1, 3 and 5 dt, with conditions similar to case II of the previous paper. Fig. 2 shows the list of reactions and the corresponding rate constants.

2.3. Reverse mapping

Computing the physical and mechanical properties for polymer glasses can be done either by atomistically detailed or by CG simulation methods. The results obtained in the past ten years show that nowadays MD simulations are mature enough to address several physical and mechanical properties, in spite of the obvious limitation in time and length scales [17]. CG methods, on the other hand, so far cannot provide quantitatively accurate predictions. Therefore, after some degradation time, we reverse map our (degraded) CG structure to a fine-grained (FG) one, as the third step of our simulation scheme.

2.4. Property calculations

In the fourth stage, we perform several MD simulations on the FG structure to obtain material properties. We briefly reviewed the first two steps of our multi-scale approach in the previous sections. In the following section, we will elaborate on the fine graining and MD methods employed in steps three and four of our multi-scale simulation approach.

$$\left.\begin{array}{ll} A-B \rightarrow A^{\bullet}+B^{\bullet} & (I-1) \\ A-\beta \rightarrow A^{\bullet}+\beta^{\bullet} & (I-2) \end{array}\right\} \textit{initiation} \qquad \begin{array}{l} K_{I-1}=\frac{1}{3}dt^{-1} \\ K_{I-2}=\frac{2}{3}dt^{-1} \end{array}$$

$$\left.\begin{array}{ll} A+B^{\bullet} \rightarrow A^{\bullet}+B & (P-1) \\ C+B^{\bullet} \rightarrow C^{\bullet}+B & (P-2) \\ A+\beta^{\bullet} \rightarrow A^{\bullet}+\beta & (P-3) \\ C+\beta^{\bullet} \rightarrow C^{\bullet}+\beta & (P-4) \\ C+A^{\bullet} \rightarrow C^{\bullet}+A & (P-5) \end{array}\right\} \textit{propagation} \qquad \begin{array}{l} K_{P-1}=K_{P-2}=\frac{1}{3}dt^{-1} \\ K_{P-3}=K_{P-4}=\frac{1}{3}dt^{-1} \\ K_{P-5}=\frac{1}{3}dt^{-1} \end{array}$$

$$\left.\begin{array}{ll} A^{\bullet}+A^{\bullet} \rightarrow A-A & (T-1) \\ B^{\bullet}+B^{\bullet} \rightarrow \beta-\beta & (T-2) \\ \beta^{\bullet}+\beta^{\bullet} \rightarrow \beta-\beta & (T-3) \end{array}\right\} \textit{termination} \qquad \begin{array}{l} K_{T-1}=\frac{1}{2}dt^{-1} \\ K_{T-2}=K_{T-3}=\frac{1}{2}dt^{-1} \end{array}$$

Fig. 2. List of reactions for photo-degradation simulations with the corresponding reaction rate constants.

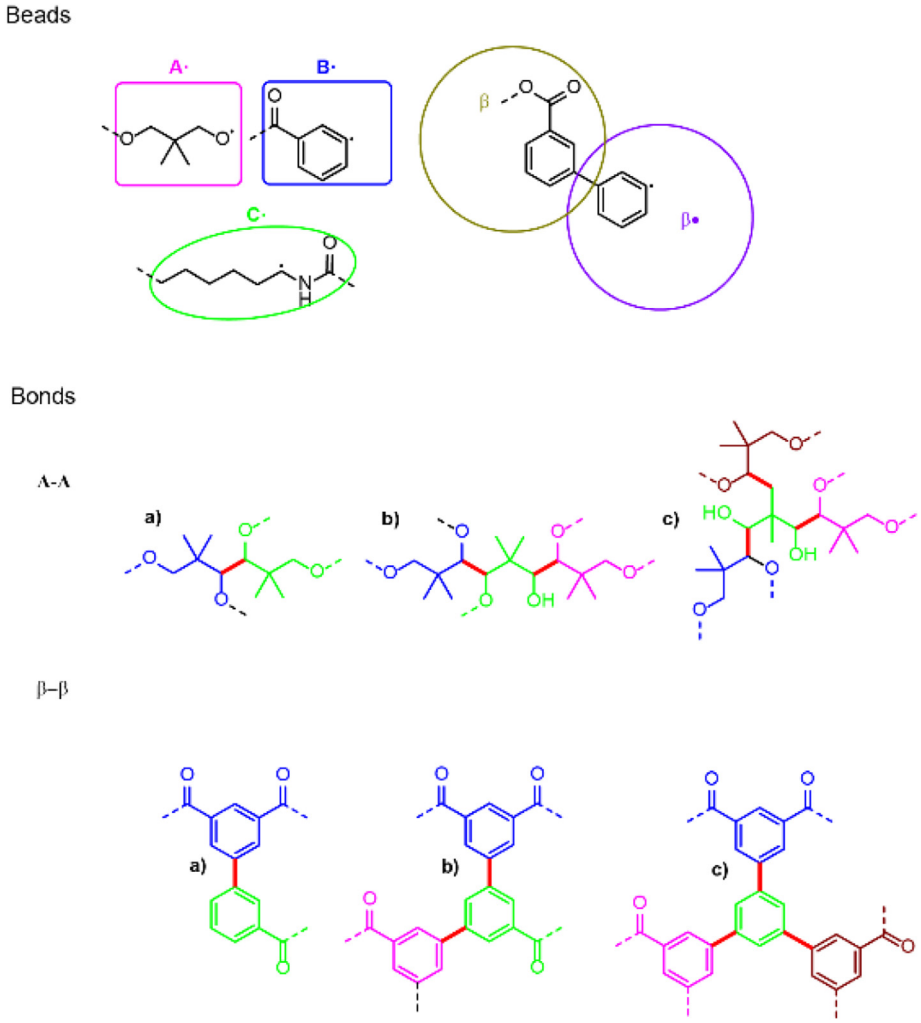

Fig. 3. Overview of new CG beads and bonds taken into account during the photo-degradation simulation.

3. Methods for establishing thermo-mechanical properties

3.1. Reverse mapping

For reverse mapping we developed an algorithm based on an existing method that has been used for an epoxy amine system [17]. Substantial modifications were needed to adopt the algorithm to our system due to the chemical changes during the photo-degradation process. A detailed description of the reverse mapping algorithm is provided in the supporting information (SI).

Essentially this procedure delivers an atomistic structure of a CG structure at any desired point in time that can be used for further MD calculations.

3.2. Molecular dynamics methods

MD simulations have been done using the LAMMPS (Large-scale Atomic/Molecular Massively Parallel Simulator) molecular dynamics code [18]. As force field, PCFF (Polymer Consistent Force Field) has been employed to parameterize the interactions between atoms [19] in a periodic box of the material, consisting of initially 114,600 atoms (virgin material).

3.2.1. Energy minimization

The first step for our MD simulations is the energy minimization and the equilibration of the material at the required temperature. This is a necessary step for most molecular simulations after a reverse mapping procedure [20,21]. Although we equilibrate the structure of the material with a DPD method at given time intervals during the photo-degradation process, in the reverse mapping process, we introduce somewhat over-stretched bonds (see SI), and therefore we first minimize the energy of the material to regain the equilibrium bond lengths between atoms. This removes the surplus potential energy stored in these bonds.

We use a Polak–Ribiere version of the conjugate gradient algorithm [22] to estimate the minimum potential energy of the material. After reaching equilibrium, as assessed from the potential energy, we start gradually increasing the temperature of the material to 500 K using a Berendsen thermostat [23]. Next, we continue with an MD equilibration step under isothermal-isobaric (NPT) conditions at 500 K for 5 ns using a Nosé-Hoover thermostat [24] and a Parrinello-Rahman barostat [25]. Eventually, we decrease the temperature to 300 K and continue the MD simulation for another 5 ns.

3.2.2. Thermal properties

We conducted stepwise temperature sweep simulations at atmospheric pressure within a range from 250 K to 500 K with 10 K steps in which we let the system relax after each temperature step for 60 ps. After such a relaxation, we always average the volume of the material over another 360 ps, using a block averaging method [26], in order to obtain volume–temperature curves. In detail, we sampled the volume of the system every 0.1 ps. For such a dataset of 3600 volumes, we perform the block averaging analysis to obtain the averaged volume of the system and the magnitude of the error of the averaged volume. The error for any averaged volume is the standard deviation of the fluctuation at that temperature step divided by the number of uncorrelated blocks.

After obtaining the volume–temperature curves, the value of T_g is obtained using a multi-phase regression as the joint point of two linear regressions on the magnitude of the volumes, below and above the transition, respectively. Furthermore, we use a Monte Carlo method to estimate the error of the fitting process using the covariance matrix of the fitting parameters for both lines [27].

All simulations have been performed with constant NPT conditions using a Nosé-Hoover thermostat and a Parrinello-Rahman barostat. Using the volume–temperature curves we computed the T_g and the coefficient of thermal expansion α of the material at four moments in time during the photo-degradation process.

3.2.3. Mechanical properties

Dynamic mechanical analysis (DMA) is a powerful tool to study experimentally the thermo-mechanical properties of polymeric coatings. Using this technique, one can distinguish between the elastic and the viscous properties of polymeric networks. Therefore, it is important to mimic such an experiment in our simulation approach, to be able to study the change in properties of the material during the photo-degradation process. We studied the change of several physical and mechanical properties of the material during photo-degradation, i.e., the storage and loss moduli (and hence tan δ), the thermal expansion coefficient α and the glass transition temperature T_g.

There are several simulation studies dealing with the change in elastic constants of polymeric thermosets during the curing process [14,21,28]. However, these studies mainly focus on the change of Young's modulus with temperature by applying a linear tensile strain. In contrast, in this study to mimic DMA, we impose an oscillatory uniaxial strain field to the polymer network and we evaluate the resulting stress. From the computed pressure tensor, one can obtain the normal stresses of the material (the diagonal components of the pressure tensor) in x, y and z directions. Fitting a sinusoidal curve on the computed normal stresses, with the same frequency as for the strain, results in the maximum stress, σ_0 and phase lag, δ. The storage modulus E' and loss modulus E'' of the material are then calculated using Equations (1) and (2), respectively.

$$E' = \frac{\sigma_0}{\varepsilon_0}\cos\delta \tag{1}$$

$$E'' = \frac{\sigma_0}{\varepsilon_0}\sin\delta \tag{2}$$

where ε_0 is the maximum strain applied. For obtaining the dynamic mechanical properties we performed oscillatory strain simulations using constant NPT conditions at different temperatures. E', E'' and tan δ were calculated at four different photo-degradation times for a temperature range from 200 K to 600 K with 50 K steps. For each simulation, after 500 ps relaxation of the material at the desired temperature, we applied one complete period of oscillation on x, y and z directions using the same strain and frequency. We averaged the results of three simulations for each temperature for more reliable statistics.

4. Results and discussion

Table 1 summarizes the number of CG bonds in the simulated polymer network at the abovementioned photo-degradation times, see Section 2. Comparing the change in the number of ester bonds in our simulation with the change in the number of ester bonds for the same material in an actual weathering experiment, one can roughly estimate a conversion factor between the number of dt units in a simulation and the experimental weathering time. Note that since our reaction rates in photo-degradation simulations are arbitrary, an exact comparison with experimental results is not possible. However, comparing preliminary FTIR results of a sample (the same material as our simulation) with 5 μm thickness placed in an Atlas Suntest XXL machine for accelerated weathering under dry nitrogen atmosphere (i.e., using a similar condition as for our simulation) indicates a decay of 15% in the concentration of ester bonds after 5500 h of photo-degradation [29]. From Table 1, we notice that such a change in the material takes place at 0.1 dt. Therefore, roughly speaking, 1 dt in our simulations corresponds to 6 years of accelerated exposure time for the material of interest.

Now that we have an overview of the chemical changes of the material and the time frame of such changes, using our reverse mapping algorithm (see SI), we generate the atomistically detailed structure of the virgin material and degraded samples and by using MD simulations we compute their thermal and mechanical properties. In the following sections, we present and discuss the results

Table 1
Number of bonds for different photo-degradation times.

Degradation time	0 dt	0.1 dt	3 dt	5 dt
A–B	4800 (100%)	4065 (85%)	1070 (22%)	696 (14.5%)
A–C	1143	1143	1143	1143
A–A	0	4	1989	2587
B–β	0	2	179	184
No. total reactions	0	1025	9953	11,415

of these MD simulations.

4.1. Glass transition temperature

Due to the change in chemical structure of the polymer network as a result of photo-degradation, one can expect changes in the thermal response of the material [30]. The most important thermal property of our clearcoat, which influences several functionalities of the coating, such as water uptake, barrier properties, etc., is the glass transition temperature T_g. Therefore, studying the change in T_g of a coating during photo-degradation is of great significance.

4.1.1. Obtaining a proper procedure

Although the method that we use to compute T_g is straightforward (inspired by dilatometry), a few considerations have to be taken into account. For instance, the heating rates that one can achieve via MD simulations (10^{14} to 10^{10} K/s) are far higher than the typical experimental heating rates (0.1–1 K/s). Note that having rates less than about 10^{10} K/s for simulations results in (unacceptably) long computation time. Moreover, the volume of the material studied in MD simulations ($\approx 10^{-21}$ cm^3) is far smaller than the experimental one ($\approx 10^{-2}$ cm^3). These differences lead to a considerable disparity between MD simulation and experimental results in the sense of absolute values. In addition, the effect of these disparities is not consistent for different polymeric materials in MD simulations. For instance, according to Soldera and Metatla, there is a linear relation between heating rate and computed T_g of various vinylic polymers [31]. In contrast, Barrat et al. show that there is a nonlinear relation between the heating rate and the T_g of polystyrene [32]. Therefore, we studied the effect of heating rate on T_g for the virgin material, although we are mainly interested in the change of the T_g as a function of photo-degradation time and any disparity in absolute value is not essential for the interpretation of our simulations.

Fig. 4 shows how the T_g of the virgin material changes as a function of heating rate during the MD simulations. Fig. 4a–c depict the volume–temperature curves of the virgin material with varying heating rates. Fig. 4d, shows the intersection of the two fitted lines to the corresponding volume–temperature curves, T_g, as computed with the method discussed in Section 3.2.2.

As expected, the computed T_g increases with heating rate and T_g varies from 407.1 to 413.3 K, when the heating rate was increased from 2.38×10^{10} to 8.33×10^{10} K/s. In addition, one notices larger error bars for the computed T_gs at higher heating rates. As also can be seen in Fig. 4, the deviation of the averaged volumes from the fitted lines (especially at temperatures above T_g) increases when the heating rates are increased. One can rationalize this effect using two arguments. First, having a higher heating rate means having less time for equilibration of the material at a specific temperature, which leads to higher inaccuracies for the averaged volumes. Second, having less time for each temperature step leads to a lower number of samples, which has an adverse influence on the statistics. This increased error also can be seen in Fig. 5a, where the coefficient of thermal expansion α for the glassy and rubbery states are plotted as a function of heating rate. The error bars (especially for the rubbery state) are larger for higher heating rates.

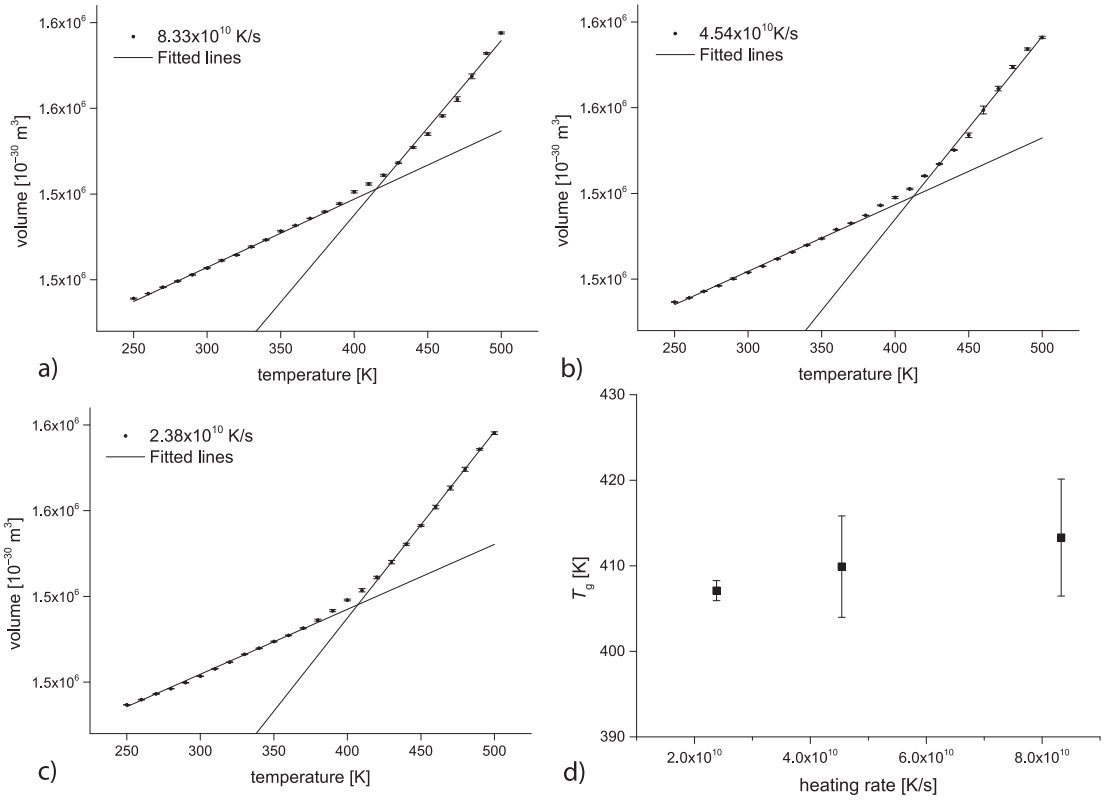

Fig. 4. a, b and c) Volume-temperature curves for virgin material at different heating rates. d) Summary of the change in T_g as a function of heating rate.

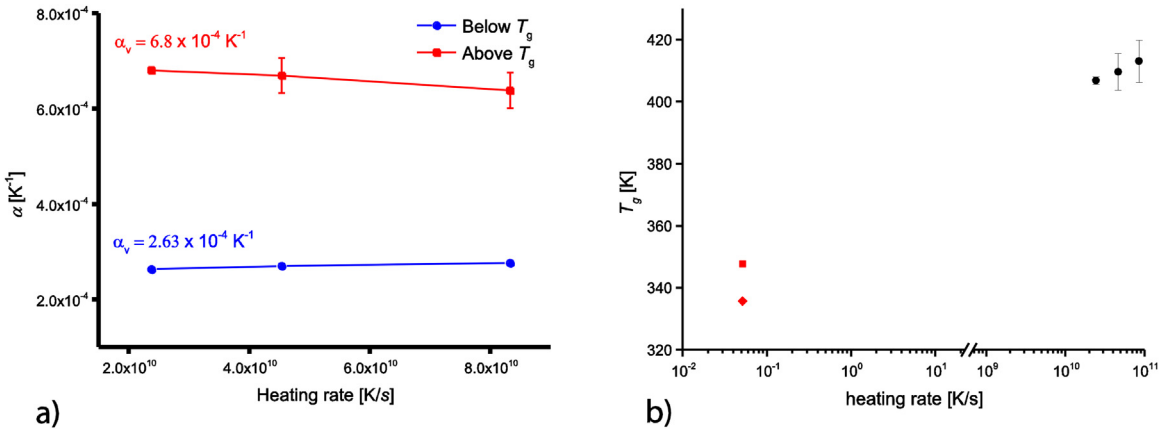

Fig. 5. a) The simulated thermal expansion coefficient α for the glassy and rubbery states as a function of heating rate. b) Comparison between experimental (red square for MDSC and diamond for DMA experiment) and simulation T_gs (black dots). (For interpretation of the references to color in this figure legend, the reader is referred to the web version of this article.)

In order to compare the computed T_g of the fresh material with the experimental values, we conducted a modulated DSC experiment using a heating rate of 0.05 K/s with a modulation of 0.5 K and 30 s, as well as a Dynamic Mechanical Analysis experiment with a heating rate of 0.05 K/s and frequency of 10 s^{-1}. The measured T_gs of 336 K for DSC measurement (indicated by the inflection point of the heat flow–temperature curve) and around 348 K for experimental DMA measurement (indicated by the peak of tan δ), are plotted in Fig. 5b, together with the simulated T_gs. The considerable difference between the simulated and experimental values is probably largely due to the significant difference in heating rates, but the absence of real long range-time relaxations in the simulations may also contribute.

4.1.2. T_g changes

So far, we established a method to compute thermal properties of the material. As we are interested in the change of these properties as a function of photo-degradation time, we employed the abovementioned method, with a heating rate of 2.38 $\times$ 10^{10} K s^{-1}, to compute the thermal properties of the degraded material, i.e., after simulated degradation for 0, 0.1, 3 and 5 dt. Fig. 6a and b depict the volume–temperature curves and the computed α and T_g of the material, respectively, at the various photo-degradation times.

As changes in the thermo-mechanical properties of the material during photo-degradation stem from chemical changes in the material as a result of photo-degradation, any rationalization of the computed values should be based on chemical changes in the system. As discussed in a previous paper [8], in a nitrogen atmosphere, the determining factors in photo-degradation chemistry are bond scission and recombination reactions. Due to the photo-oxidative nature of urethane bond scission [33], in our photo-degradation simulation we do not break urethane bonds photolytically (the number of urethane bonds remains constant during photo-degradation, see Table 1) and bond scission takes only place at ester bonds, see Fig. 3 reactions I-1 and I-2. In order to have a better view on the most important chemical changes, i.e., ester bond scission and recombination reactions, we made a few images of CG material after the degradation times of interest.

Fig. 7 shows the distribution of aliphatic, aromatic and cross-linker beads, and the corresponding bonds for the virgin material. At 0 dt, no bonds between pairs of A and pairs of B beads exist, see Fig. 7a and b. However, all A and B beads are connected to one or two other beads of the opposing type by an ester bond with a homogenous distribution over the simulation volume, see Fig. 7c. The distribution of the cross-linker is also homogeneous, as Fig. 7d shows.

Fig. 8a and b depict the evolution of A–A and B–B bonds during photo-degradation. As shown and already indicated in Table 1, at about 0.1 dt new crosslinks start to form, and the number of recombination reactions accelerates in such a way that at very long

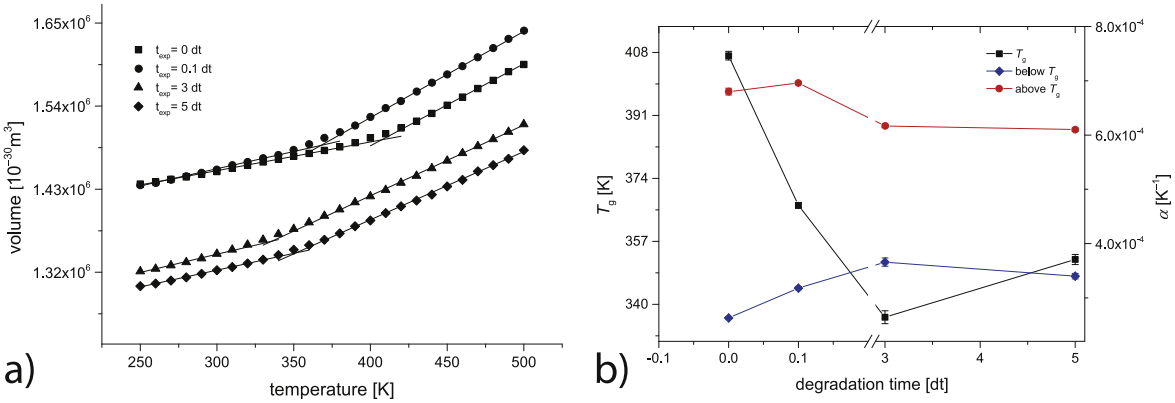

Fig. 6. a) Volume-temperature curves at 0, 0.1, 3 and 5 dt b) T_g and α (below and above T_g) as a function of photo-degradation time. The time axis of the right figure is broken between 0.2 and 2.9 dt for easier visualization. The lines are drawn to guide the eye.

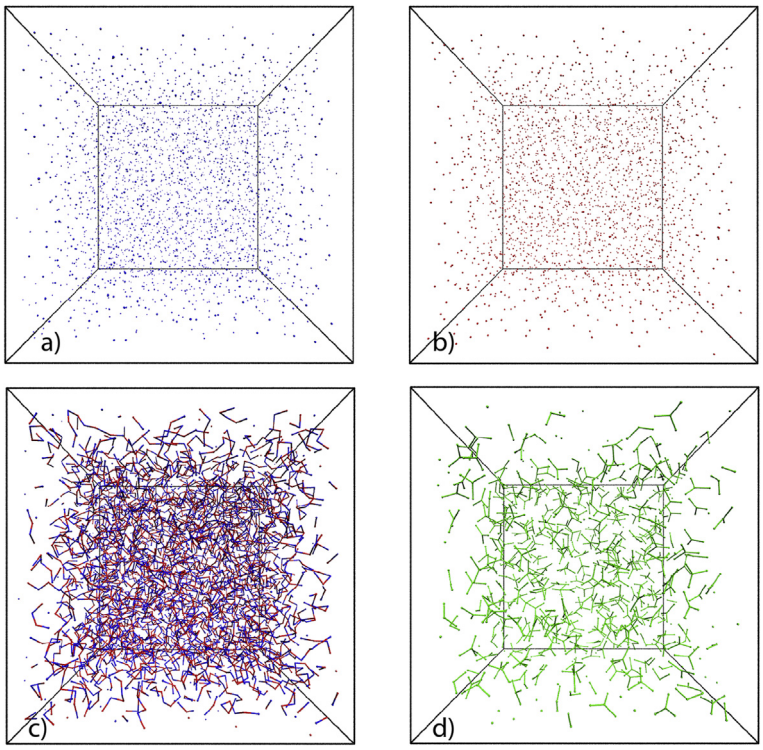

Fig. 7. The spatial distribution of beads in virgin material (at 0 dt). a) Aliphatic beads (A bead), b) aromatic beads (B), c) ester bonds (A–B), d) cross-linker molecules (C, D and E beads).

degradation times the network connectivity is preserved, although many ester bonds are broken. However, due to the enormous number of broken ester bonds (Fig. 9), one can notice some unconnected beads freely floating through the network (unconnected beads at the edge of the box are not free since the periodic bonds are removed for easier visualization).

Now we look back at Fig. 6, where the changes in T_g and α are shown. As already mentioned, at 0.1 dt almost no recombination reactions took place and the main change in the chemistry is due to ester bond scission (15% of the initial number of ester bonds are

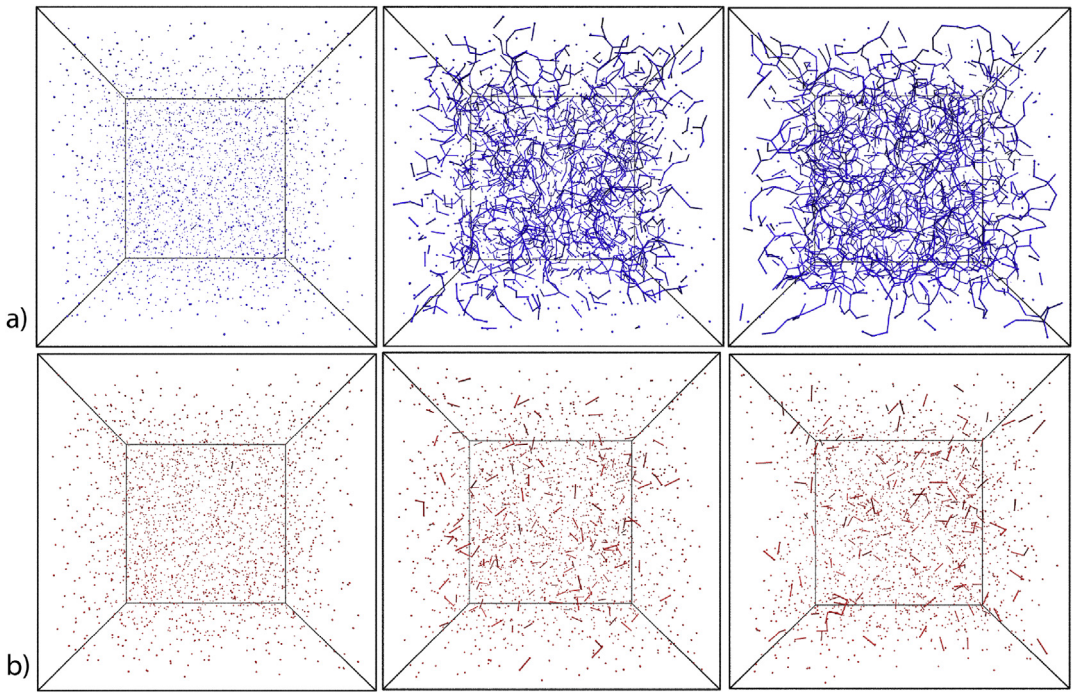

Fig. 8. The evolution of cross-links at 0.1, 3 and 5 dt (from left to right), respectively. a) A–A (aliphatic cross-links), b) B–B (aromatic cross-links).

broken, see Table 1). This explains the drop in T_g and the slight increase in α above the T_g as one expects, first, that a looser network of material has a lower T_g and, second, one expects a higher α value in the rubbery state due to a decreasing network connectivity. Although the opposite effect for both T_g and α in the rubbery state has been observed in a simulation study for an epoxy system as a function of cross-linking conversion [34], this in fact supports our observation because in that case the cross-link density is increasing instead of decreasing.

Extending the degradation time further up to 3 dt and looking at Table 1, we see that, although ester bond scission has been taking place, recombination reactions occurred at the same time, between 0.1 dt and 3 dt. These opposing effects result in a further decrease of the T_g of the material, but only a slight decrease of α in the rubbery state. In this interval of photo-degradation time, it is difficult to directly correlate the chemical changes to changes in the network structure of the material and eventually to thermal properties. As can be seen in Fig. 8, on one hand, recombination reactions increase the cross-link density of the system and, on the other hand, ester bond scission decreases the cross-link density of the system. What we observe, is a combination of these opposing effects.

With prolonged photo-degradation, up to 5 dt, the decrease in the number of ester bonds, as compared to 3 dt (371 ester bonds were broken between 3 and 5 dt), is less pronounced than the recombination reactions (698 recombination reactions took place between 3 and 5 dt). This results in a slightly higher T_g of the material, as compared to 3 dt and almost no change in α in the rubbery state. It is also worth noticing that recombination reactions introduce inhomogeneity in the network structure (Fig. 9). In other words, the cross-links are no longer uniformly distributed over the system anymore, as they were in the virgin material, see Fig. 7d. This phenomenon, at larger scale, might lead to spatial inhomogeneity of the network which could facilitate defect creation and ultimately cracking of the coating.

4.2. Dynamic mechanical analysis

Similar as for the T_g, we first discuss the procedure used and thereafter the modulus changes.

4.2.1. Obtaining a proper procedure

Performing dynamic mechanical simulations for a series of temperatures allows one to obtain E', E'' and tan δ as a function of temperature. Although this method seems straightforward, there are several complications as a result of stress fluctuations, due to the small system size and the limited simulation time. Therefore, in order to minimize the uncertainties in the computed stress, a larger amplitude can be used to improve the signal-to-noise ratio. However, one should not exceed the limit of linear viscoelastic response of the material. In order to make sure that our simulations remain in the linear region, we performed a set of strain sweep tests. Fig. 10a–c shows how the signal-to-noise ratio changes with strain and Fig. 10d depicts the change in the computed E' and E'' as a function of strain.

Experimentally, a maximum strain of 2–3% is often larger than the maximum of the linear-viscoelastic region of typical highly-crosslinked polymers. As Fig. 10d shows, for our simulations the mechanical properties of the material do not change systematically using a maximum strain of up to 0.0345. This is an indication that we are still in the linear region. Nevertheless, for temperatures below T_g, we apply a maximum strain of 0.0216 to ensure linearity. For temperatures higher than T_g, the material becomes softer and the moduli drop significantly. Therefore, in order to have an acceptable signal to noise ratio for the computed stresses, we use 0.0345 for the maximum strain above T_g.

Another factor is frequency. On the one hand, lower frequencies are closer to experimental frequencies, thus will give rise to more realistic results, with a higher chance for less correlated sampling. On the other hand, lower frequencies need longer simulation times. In order to test the effect of frequency on the mechanical properties, we performed a set of simulations with 0.0216 strain at 300 K (at which the material is in a glassy state) with different frequencies, i.e., 4×10^9, 7.27×10^8, 4×10^8 and 2×10^8 s^{-1}.

Fig. 11 shows the phase lag between stress and strain changes with changing frequency. A lower frequency results in a larger phase lag between stress and strain at constant temperature, meaning that the behavior of the material becomes less elastic and the viscous component in the response increases with decreasing frequency. According to the time–temperature superposition principle [35], lowering the frequency at constant temperature has the same effect as increasing the temperature at constant frequency. Experimentally, increasing the temperature of a glassy material gives rises to a lower storage modulus and a higher damping factor. Fig. 11 emphasizes the presence of a similar effect in our simulation results.

In order to test the effect of the frequency of the simulation on the mechanical behavior of the material as a function of temperature, we performed a set of simulations in the temperature range from 250 K to 600 K with 50 K steps for the virgin material with different frequencies (4×10^9, 7.7×10^8 and 4×10^8 s^{-1}). We combined the computed storage moduli, E', of our simulations and the values from Dynamic Mechanical Analysis (DMA) experiments

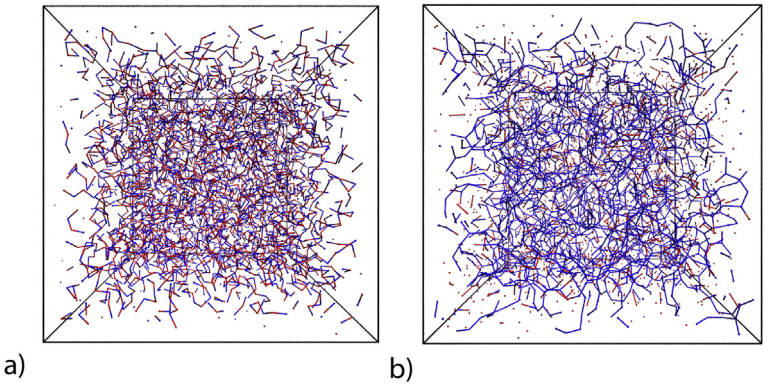

Fig. 9. Network structure changes from a well-defined structure, Fig. 9a at 0 dt, consisting of ester bonds (half red half purple bonds) and urethane bonds (removed in these figures for easier visualization), to a more heterogeneous structure, Fig. 9b at 5 dt, in which the majority of the connections are newly formed A–A and β–β bonds (full blue or full red, respectively) instead of initially existing ester bonds. (For interpretation of the references to color in this figure legend, the reader is referred to the web version of this article.)

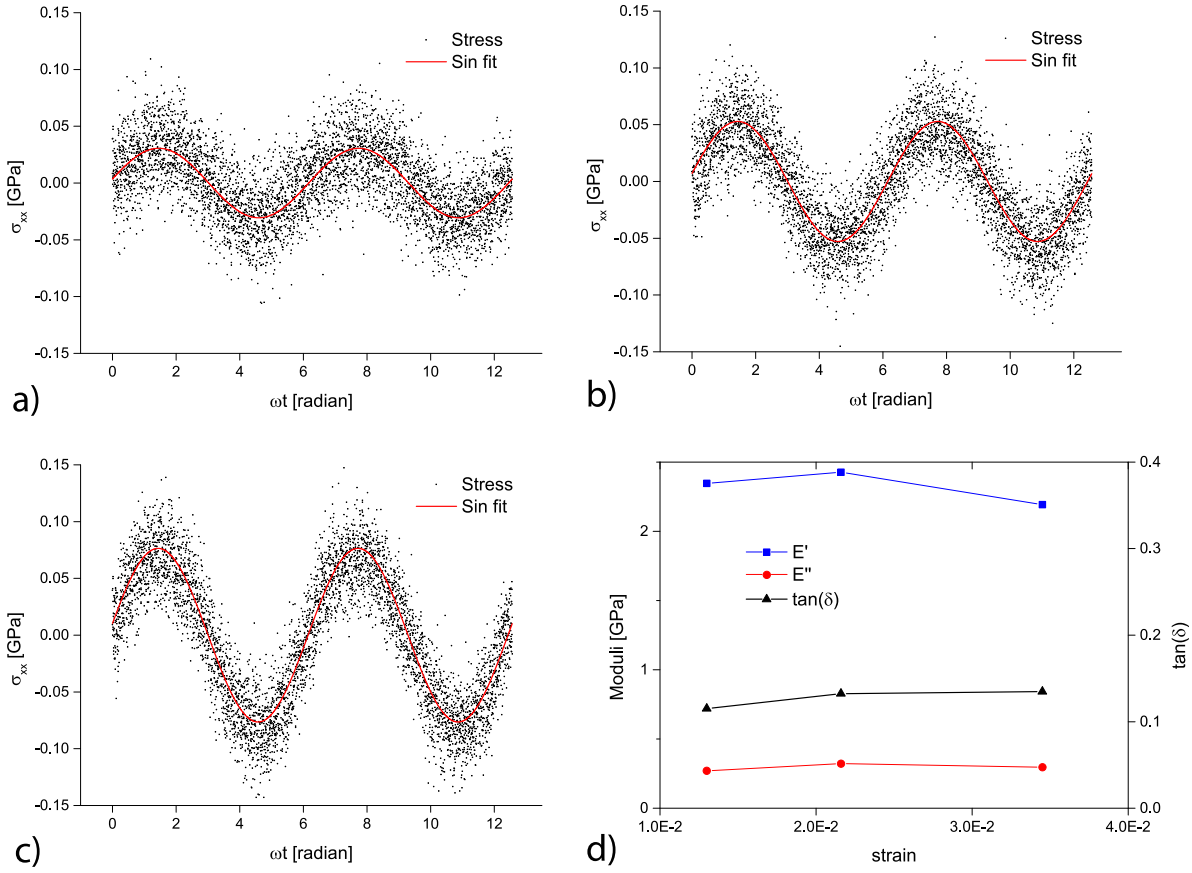

Fig. 10. The change in the signal-to-noise ratio as a function of strain at 300 K. For maximum strains of 0.013 (a), 0.0216 (b), and 0.0345 (c). d) Mechanical properties as a function of strain.

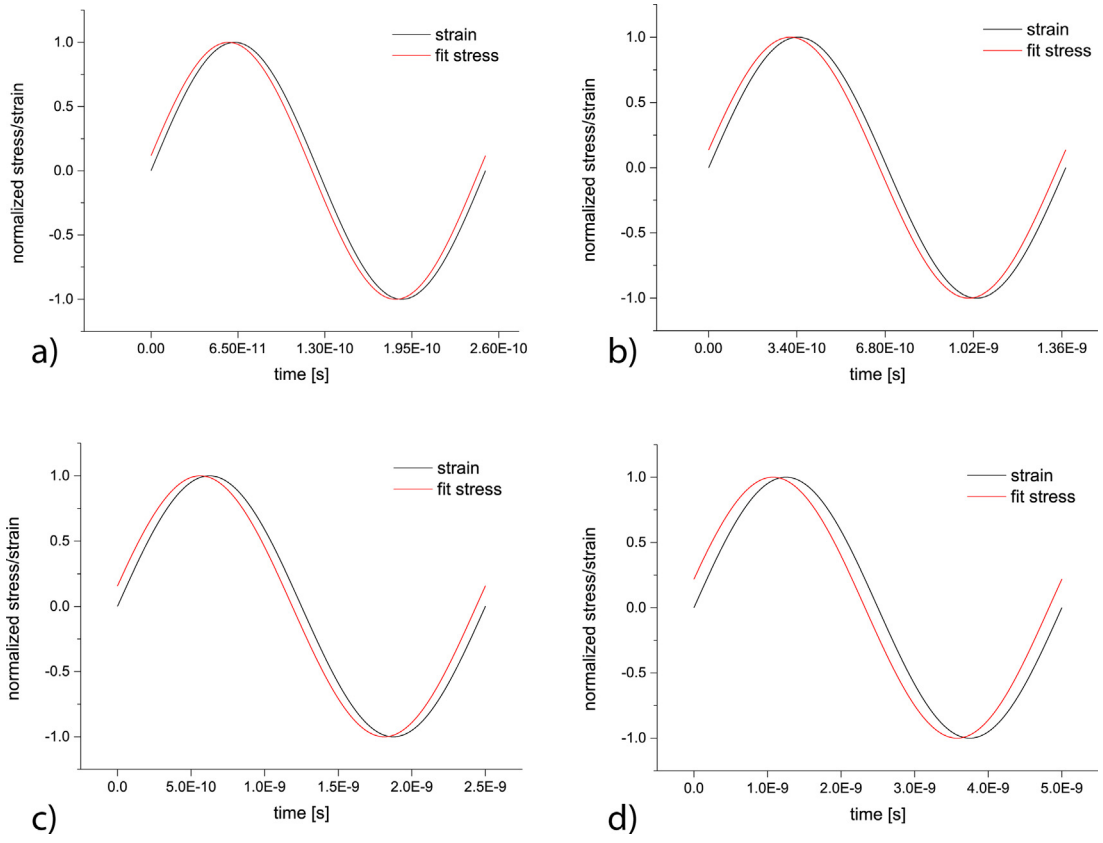

Fig. 11. Normalized stress and strain curves as a function of simulation time at different frequencies. The frequencies are 4×10^9, 7.27×10^8, 4×10^8 and 2×10^8 s^{-1} for a, b, c and d, respectively.

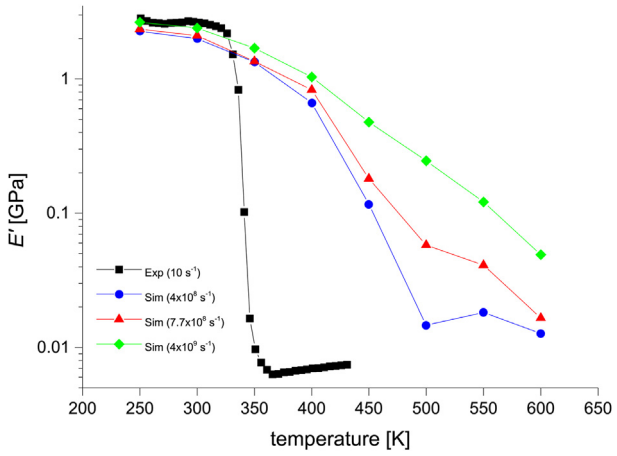

Fig. 12. E' of the virgin sample as a function of temperature at 4 frequencies: 4×10^9, 7.27×10^8, 4×10^8 and 10 s^{-1}. The results corresponding to frequency 10 s^{-1} are obtained experimentally.

in Fig. 12.

As shown, varying the frequency changes the values of E' as a function of temperature. Sirk et al. have observed the same effect for the Young's modulus of an epoxy network in their simulation study [36]. This effect is also in line with the time–temperature superposition principle, as one can notice that at higher frequencies and in the same range of temperatures, longer relaxation times cannot be captured; therefore a higher temperature is needed to cover the transition zone. Having said that, a noticeable feature is the large width of the transition zones that we observed in our simulations as compared to the experimental values. Lowering the frequency decreases the width of the transition, but for the lowest simulated frequency it is still wide. Lowering this frequency any further is not feasible because the excessive computer power required. At a frequency of 4×10^8 s^{-1}, 2.5 million time steps with a relatively large time step of 1 fs are needed for a single oscillation period. All in all, in order to study the effect of photo-degradation on the material, we use the frequency 4×10^8 s^{-1} and we will focus on qualitative changes.

4.2.2. Modulus changes

After having established a proper procedure for dynamic mechanical simulations using the virgin material, and resulting in a maximum strain of 0.0216 and 0.0345 below and above T_g, respectively, at a frequency of 4×10^8 s^{-1}, we perform simulations with the same parameters for all samples. Fig. 13a and b depict the changes in E', E'' and tan δ as a function of temperature for the virgin material, i.e., at 0 dt, as obtained by simulation and experiment, respectively. As expected, a steep drop for E', a peak for E'' and a peak for tan δ as a function of temperature are present, indicating the glass transition. The sequence of these changes occurs in the same way as experimentally, i.e., first E' drops sharply, thereafter the peak of E'' is found. When increasing the temperature somewhat further, we see a peak in tan δ.

Apart from elastic parameters, another important parameter for studying the network structure of cross-linked coatings during the photo-degradation process is the cross-link density. A well-known method, based on the theory of rubber elasticity, relates the value of the plateau of E' at rubbery state to the averaged cross-link density [37]. Therefore, it is interesting to see whether we can use this method also in our simulations. From Table 2, comparing the levels of E' below and above T_g, for the simulation and experimental results, one notices a good agreement between them. As expected, the offset between simulation and experiment in the rubbery state ($\approx$57%) is larger, as compared to the glassy state ($\approx$10%), due to the longer relaxation time of the material in this state. Regarding the plateau of E'' below T_g, there is 87% deviation between simulation and experiment. Also, in the temperature range of our simulations, the expected rubbery plateau of E'' did not appear. As shown in Fig. 13b, the plateau in E'' shows up at a higher temperature as for E'. Additional simulations, either at higher temperature or at lower frequency, might be able to reach the region where the plateau levels off to its final value. The broader tan δ peak found in the simulation is also a result of broadening of the other signs of transitions, i.e., E' drop and E'' peak. All in all, in our simulations we observe the same trends for E', E'' and tan δ, as observed in the DMA experiments, with the difference that all three properties show a broader glass transition zone, which is most likely due to the very high frequency of the simulations.

Having compared the simulation and experimental results of the virgin material, we next discuss the simulation analysis of degraded material. Fig. 14, shows the change in E', E'' and tan δ, respectively, in the temperature range of 200–600 K for the material after 0, 0.1, 3 and 5 dt of degradation.

Two major trends can be observed for the whole series of samples: i) the temperature range at which the transitions take place changes with photo-degradation time and ii) the steepness of the transitions varies as a function of photo-degradation time. Besides, there is specific information one can obtain by comparing E', E'' and tan δ for different photo-degradation times. For instance, comparing the graphs in Fig. 14a, one notices that the levels of the

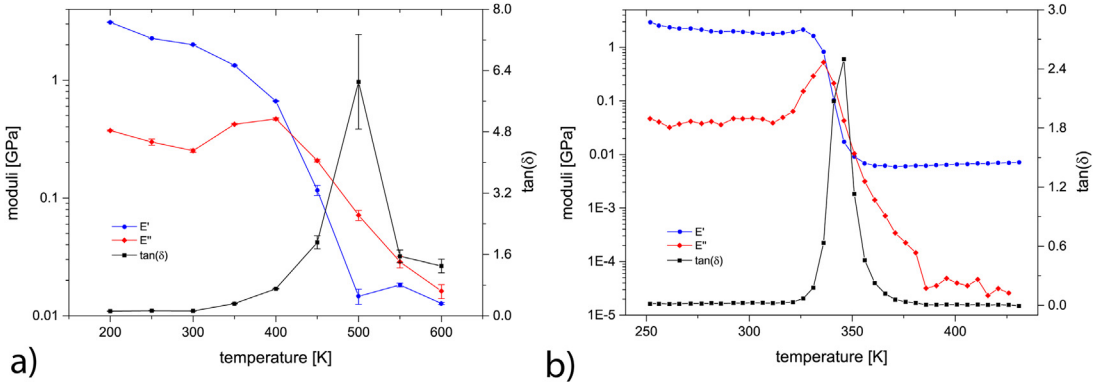

Fig. 13. Thermo-mechanical properties (E', E'' and tan δ) of the virgin material. a) Simulation results, b) experimental results. The moduli axes (left axis for both figures) are in log scale.

Table 2
Comparison between experiment and simulation for the storage and loss moduli plateau values in glassy and rubbery states of the virgin material.

Moduli	Experiment		Simulation	
	Glassy	Rubbery	Glassy	Rubbery
E' [GPa]	1.92	6.5×10^{-3}	2.13	1.51×10^{-2}
E'' [GPa]	4.10×10^{-2}	3.83×10^{-5}	3.082×10^{-1}	–

plateaus for E' in the rubbery state are slightly different. Most straightforwardly, comparing the plateau levels for the material at 0 dt (0.0151 GPa) and 0.1 dt (0.0081 GPa) nicely indicates the slight decrease in the cross-link density of the material, as also indicated by the data in Table 1. Making the same comparison for more degraded samples, however, is challenging. Due to the broadening of the transition zone as a result of photo-degradation, reaching the rubbery plateaus for 3 and 5 dt requires simulations at higher temperatures. As velocities of atoms are larger at higher temperatures, smaller MD time steps are required. As a consequence, for 600 K in the case of the most degraded sample, i.e., 5 dt, with a time step of 0.4 fs, one period of a DMA experiment could not be fully simulated. Nevertheless, one can observe the onset of the rubbery plateau to some extent for the 3 dt graph at about 0.013 GPa. This value is higher than for 0.1 dt, due to the recombination reactions that have taken place between 0.1 and 3 dt, but slightly lower than the plateau of the virgin material (0.0151 GPa).

Fig. 14b and d shows E'' as a function of temperature for all samples in log and linear scales, respectively. Fig. 14d also includes the volume–temperature curves that have been obtained from the thermal simulations (Section 3.1) with a remarkably good correlation between thermal and dynamic mechanical simulations, considering the fact that they probe the material in an entirely different way. In addition, the shift of the E'' peak is nicely in line with the shift of the intersection points of the volume–temperature curves.

From Fig. 14a and c, one notices a clear broadening of the transition zone as a function of photo-degradation time for both E' and tan δ. Lowering and broadening of the tan δ peak with photo-degradation time indicates the formation of inhomogeneities in the network structure as a result of photo-degradation. Moreover, the peaks of tan δ shift to lower temperatures as another confirmation for the thermal simulation results that show a drop in T_g (from 0 dt up to 3 dt) and slightly increasing after 3 dt. Note that the temperature resolution of dynamic mechanical simulations is 50 K and that therefore one cannot distinguish significantly smaller changes in T_g.

5. Conclusions

We developed a multi-scale simulation approach by which one can mimic the complete experimental procedure to study the effect of photo-degradation on polymeric coatings by extending a previous study [8]. By developing a three-stage simulation scheme, with widely different time and length scales involved, i.e., i) sample preparation, ii) photo-degradation and iii) thermo-mechanical analysis, and interconnecting these three stages via intermediate simulation steps using our reverse mapping method, we successfully studied the chemical and thermo-mechanical changes of a polyester-urethane coating as a result of photo-degradation. The

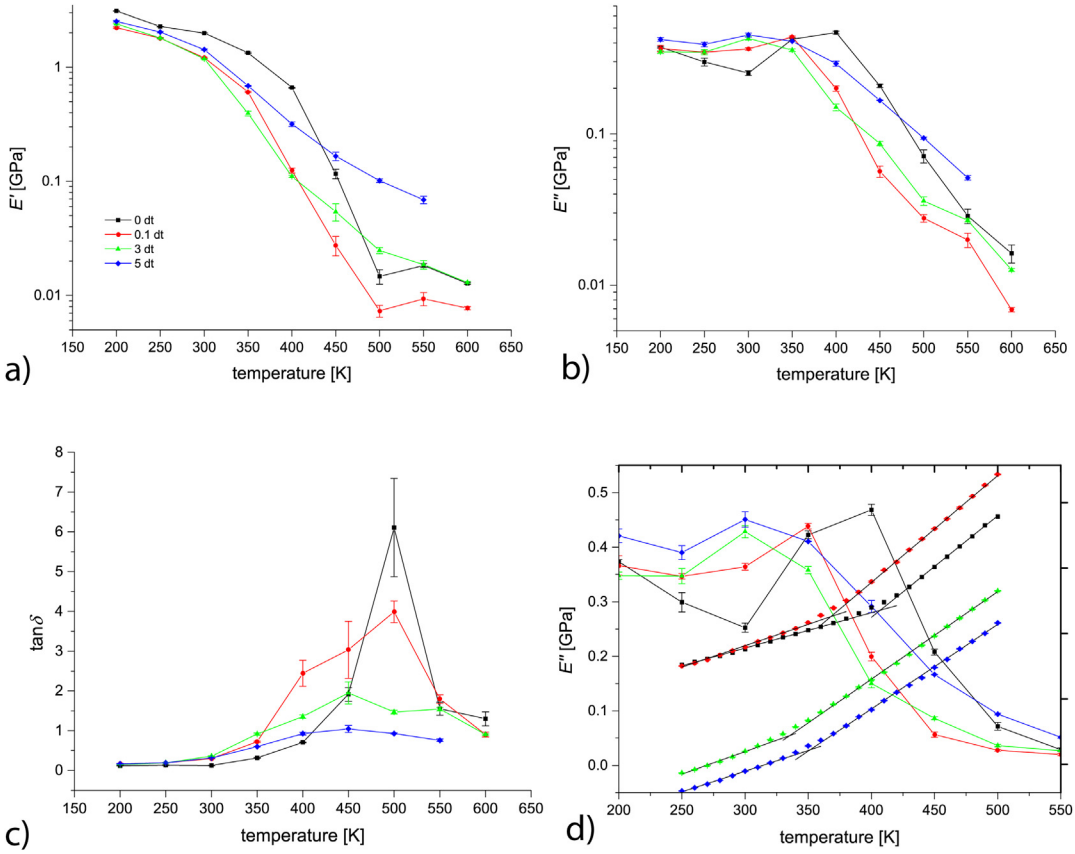

Fig. 14. Computed mechanical properties of the material during photo-degradation process at 0, 0.1, 3 and 5 dt a) E', b) E'' and c) tan δ as a function of temperature. The y-axes of a and b are shown in log scale. d) E''-temperature and volume–temperature curves.

preceding steps, i.e., KMC and DPD to obtain degraded compositions and structures [8], are essential in order to be able to assess thermo-mechanical properties with MD simulations using degraded structures. As far as we are aware of, a multi-scale simulation, like the present one covering several length and time scales as well as the resulting physical properties, as a whole has not been published before.

From the thermo-mechanical simulations, we observed a decrease in the cross-link density of the system in the initial stage of photo-degradation. Extending the photo-degradation time beyond this initial stage, we found that the decrease in cross-link density slows down and even further in time, the cross-link density slightly increases again. At the same time, the network structure becomes more inhomogeneous as a result of recombination reactions. Regarding the glass transition of the material, we observed a remarkable consistency between the results of thermal simulations and dynamic mechanical simulations for all stages of the photo-degradation process. This nicely shows how two these different test methods show a similar relaxation behavior for our material. All in all, the results of this paper demonstrate how a computational study, although using arbitrary reaction rates under anaerobic conditions, can substantially contribute to obtaining insights into the mechanisms of the photo-degradation. A study of the more complex case of photo-degradation under aerobic conditions is in progress.

Finally, we note that the procedure used is of a generic nature, i.e., it can be used for other multi-scale problems as the method is capable of correlating chemical changes of a material to changes in physical properties for processes that occur at different length and time scales.

Acknowledgment

This research forms part of the research program of the Dutch Polymer Institute (DPI), project #713.

Appendix A. Supplementary data

Supplementary data related to this article can be found at http://dx.doi.org/10.1016/j.polymdegradstab.2015.11.005.

References

[1] H. Makki, K.N.S. Adema, E.A.J.F. Peters, J. Laven, L.G.J. van der Ven, R.A.T.M. van Benthem, G. de With, Polym. Degrad. Stab. 121 (2015) 280–291.
[2] K.N.S. Adema, H. Makki, E.A.J.F. Peters, J. Laven, L.G.J. van der Ven, R.A.T.M. van Benthem, G. de With, Polym. Degrad. Stab. 110 (2014) 422–434.
[3] J.L. Gerlock, D.F. Mielewski, D.R. Bauer, Polym. Degrad. Stab. 20 (1988) 123–134.
[4] P. Malanowski, R.A.T.M. van Benthem, L.G.J. van der Ven, J. Laven, S. Kisin, G. de With, Polym. Degrad. Stab. 96 (2011) 1141–1148.
[5] D.R. Bauer, Polym. Degrad. Stab. 69 (2000) 307–316.
[6] S.G. Croll, B.R. Hinderliter, Surf. Coat. Int. Part B Coat. 88 (2005) 177–183.
[7] S. Kiil, J. Coat. Technol. Res. 9 (2012) 375–398.
[8] H. Makki, K.N.S. Adema, E.A.J.F. Peters, J. Laven, L.G.J. van der Ven, R.A.T.M. van Benthem, G. de With, Polym. Degrad. Stab. 105 (2014) 68–79.
[9] D.F. Mielewski, D.R. Bauer, J.L. Gerlock, Polym. Degrad. Stab. 33 (1991) 93–104.
[10] D.R. Bauer, Polym. Degrad. Stab. 48 (1995) 259–267.
[11] D.R. Bauer, Prog. Org. Coat. 23 (1993) 105–114.
[12] D.R. Bauer, J.I. Gerlock, D.F. Mielewski, M.C.P. Peck, R.O. Carter, Ind. Eng. Chem. Res. 30 (1991) 2482–2487.
[13] J.-F. Larché, P.-O. Larché, J.-L. Gardette, Polym. Degrad. Stab. 95 (2010) 1810–1817.
[14] F. Bénard, B. Mailhot, J. Mallégol, J.L. Gardette, Polym. Degrad. Stab. 93 (2008) 1122–1130.
[15] G. Rossi, I. Giannakopoulos, L. Monticelli, N.K.J. Rostedt, S.R. Puisto, C. Lowe, A.C. Taylor, I. Vattulainen, T. Ala-Nissila, Macromolecules 44 (2011) 6198–6208.
[16] G. Kacar, E.A.J.F. Peters, G. de With, Epl Europhys. Lett. (2013) 102.
[17] G. Kacar, E.A.J.F. Peters, G. de With, Comput. Mater. Sci. 102 (2015) 68–77.
[18] S. Plimpton, J. Comput. Phys. 117 (1995) 1–19.
[19] H. Sun, S.J. Mumby, J.R. Maple, A.T. Hagler, J. Am. Chem. Soc. 116 (1994) 2978–2987.
[20] S.O. Nielsen, R.E. Bulo, P.B. Moore, B. Ensing, Phys. Chem. Chem. Phys. 12 (2010) 12401–12414.
[21] P.V. Komarov, Y.T. Chiu, S.M. Chen, P.G. Khalatur, P. Reineker, Macromolecules 40 (2007) 8104–8113.
[22] E. Polak, G. Ribière, Rev. Fr. Inf. Rech. O 3 (1969) 35–43.
[23] H.J.C. Berendsen, J.P.M. Postma, W.F. van Gunsteren, A. Dinola, J.R. Haak, J. Chem. Phys. 81 (1984) 3684–3690.
[24] S. Nosé, J. Chem. Phys. 81 (1984) 511–519.
[25] M. Parrinello, A. Rahman, J. Appl. Phys. 52 (1981) 7182–7190.
[26] A. Grossfield, D.M. Zuckerman, Annu. Rep. Comput. Chem. 5 (2009) 23–48.
[27] A. Ganse, A Brief Lowdown of "Multi-Phase Linear Regression" http://staff.washington.edu/aganse/mpregression/mpregression.html.
[28] N.B. Shenogina, M. Tsige, S.S. Patnaik, S.M. Mukhopadhyay, Macromolecules 45 (2012) 5307–5315.
[29] H. Makki, Modelling and Physical Study of Weathering Opf a Polyesterurethane Coating (PhD thesis), Eindhoven University of Technology, 2015.
[30] J.D. Menczel, R.B. Prime, Thermal Analysis of Polymers, Fundamentals and Applications, John Wiley & Sons, 2009.
[31] A. Soldera, N. Metatla, Phys. Rev. E (2006) 74.
[32] J.L. Barrat, J. Baschnagel, A. Lyulin, Soft Matter 6 (2010) 3430–3446.
[33] C. Wilhelm, J.-L. Gardette, Polymer 38 (1997) 4019–4031.
[34] S.R. Yang, J.M. Qu, Polymer 53 (2012) 4806–4817.
[35] M.L. Williams, R.F. Landel, J.D. Ferry, Phys. Rev. 98 (1955), 1549–1549.
[36] T.W. Sirk, K.S. Khare, M. Karim, J.L. Lenhart, J.W. Andzelm, G.B. McKenna, R. Khare, Polymer 54 (2013) 7048–7057.
[37] A. Skaja, D. Fernando, S. Croll, J. Coat. Technol. Res. 3 (2006) 41–51.